AIAA JOURNAL
Vol. 38, No. 9, September 2000

Modeling of Afterbody Flows with Realistic Propulsive Gases: A Prospective Study

Richard Benay* and Patrick Servel†
ONERA, F-92190 Meudon, France

The organization of afterbody flows of missiles or launchers determines the base pressure, which is itself a key factor influencing the thrust budget. The structure of the afterbody is submitted to aerothermal loads due to the mixing of the external flow with the high-temperature gases exiting from the nozzle. The general feature of the afterbody flow, determining energy transport phenomena, directly influences the thermal fluxes to which the structure is submitted. The importance of establishing precise methods of calculation to predict transport phenomena in the mixing of realistic gaseous species appears now at the design level. To realize this program, fundamental works on afterbody flows have been performed in the field of modeling, where the NASCA code was developed for these purposes, and also in the experimental field, where data benchmarks were constituted for cold supersonic flows. For the case of realistic temperature and chemical compositions, benchmarks do not currently exist, and the aim is to establish a model of transport phenomena in nonreacting multicomponent gases that is consistent with the more commonly used turbulence models. After validating the code on a reference configuration with supersonic cold flow and a cold propulsive jet, prospective calculations are performed with more realistic high-temperature jet conditions and chemical compositions. Some divergences between the model's predictions of aerothermal fields are observed.

Nomenclature

C_p, $\hat{C}_p$, C_{pi}	= heat capacities at constant pressure
C_v, C_{vi}	= heat capacities at constant volume
D_i, D_T, D_{ij}	= molecular, turbulent, and binary diffusion coefficient
e	= energy
e_s	= sensible internal energy
h, h_i	= enthalpies
h_s	= sensible enthalpy
k	= turbulent kinetic energy
Le, Le_T	= molecular and turbulent Lewis numbers
m_i	= molar masses
P, P_t, P_{tj}	= pressure: static, total (or stagnation), total of the jet
Q_i^0	= heats of formation
$\Re$	= constant of perfect gases
T, T_t, T_{tj}	= temperature: static, total (or stagnation), total of the jet
u_i	= velocities
u_i''	= turbulent fluctuation of velocities
$\boldsymbol{V}_m$, V_m^i	= mean velocities of species m
x_m	= mole fraction of species m
y_m	= mass fraction of species m
γ, $\hat{\gamma}$	= ratios of specific heats (classical and generalized)
$\bar{\varepsilon}$, ε	= internal energy, turbulent dissipation
λ, λ_T	= molecular and turbulent thermal conductivities
μ, μ_T	= molecular and turbulent viscosities
ρ	= density
τ_{ij}, τ_{ij}^T	= molecular and turbulent shear stresses
ω_m	= chemical source term of species m

I. Introduction

THE flow confluence occurring downstream of missile afterbodies induces complex aerothermochemical phenomena due to the composition of the high-temperature gases constituting the propulsive jet, exiting the combustion chamber and mixing with the external stream. These two coflowing streams involve a recirculating zone where the mixing between the various gases takes place. The aerodynamic state of this recirculation bubble, because it directly touches the base of the afterbody, determines the pressure on it and, thus, the drag of the afterbody part of the missile. Any instability or extension of this low-speed fluid at a high temperature can have detrimental effects on the external structure and reduce the efficiency of the control surfaces near the base. Furthermore, the temperature of the gas in the recirculating bubble directly influences the heat transfers at the base and, therefore, the thermal load to which the missile bottom is submitted. The thermal aspects of the base flows then constitute a key factor, particularly for the resistance of the structure. The heat transfer is particularly increased when the propulsive gas burns or reacts with the oxygen from the external airflow in the recirculating bubble. Finally, these high-temperature gases that envelop the missile afterbody make it vulnerable to infrared detection.

During the past 20 years, missile and launcher designers have had to take into account growing major requirements in the development phase. The first, due to the progress of experimental and numerical simulations, is accuracy. A precise aerodynamic performance requirement is imposed on the engines, which implies the possession of prediction methods resulting in detailed knowledge of the phenomena. The second requirement stems from external economical constraints, such as concurrence or cost reduction, and leads to modeling methods with criteria of low costs and speed. In this perspective, computational fluid dynamics (CFD) methods have quickly become the object of particular attention. However, this approach to the problem includes an important experimental side. Improving general predictive calculation methods for future use implies their validation in a certain number of fundamental, well-chosen, and defined cases. The preparation of the fundamental experimental cases, the realization of experiments in small-scale facilities, the parallel implementation of CFD codes, and their validation on data benchmarks issued from the experiments constitute an essential methodology to attain the objectives stated. This methodology was used in the past to improve modeling and to validate codes in purely aerodynamic conditions with cold air jets.[1–3]

In fact, in view of the constraints just discussed, we limited our studies to axisymmetric configurations that have a sufficient degree of physical generality to accurately test a theoretical model before

Received 7 December 1998; revision received 1 September 1999; accepted for publication 29 September 1999.

*Head, Database/Theoretical Exploitation, Experimental/Fundamental Aerodynamics Department.

†Research Scientist, Experimental/Fundamental Aerodynamics Department.

its extension to three-dimensional situations. The different steps of the program were performed with the Navier–Stokes code NASCA and extend to include flows with realistic chemical compositions.[4] This analysis represents a propulsive jet in its first phase, which is the study of pure diffusion without possible postburning in the recirculating bubble. The lack of experimental data for such flows at the present time, whose realization implies the use of measurement techniques still in development, means that the theoretical studies presented in this paper are prospective in nature.

II. Theoretical Model

Balance Equations

We consider the mixing of N gaseous species indexed by i, each gas having a proper enthalpy given by

$$h_i = Q_i^0 + \int_0^T C_{pi}\,\mathrm{d}t$$

where Q_i^0 is the heat of formation at 0 K, and C_{pi} and C_{vi} are the heat capacities at constant pressure and constant volume, both being functions of the temperature. C_{pi} is established as a polynomial function of temperature.[5] The density of the gases composing the flows, sufficiently low to be considered as perfect gases, obey the classical state equation (without virial effects). Thus, we can write for the total enthalpy of the mixing

$$\rho h = \sum_i \rho_i h_i = \rho \sum_i y_i h_i = \rho \sum_i y_i \left[\int_0^T C_{pi}\,\mathrm{d}t + Q_i^0 \right]$$

$$= \rho \sum_i y_i \left[\int_0^T \left(C_{vi} + \frac{\Re}{m_i} \right) \mathrm{d}t + Q_i^0 \right]$$

$$= \rho \sum_i y_i \left[\int_0^T C_{vi}\,\mathrm{d}t + Q_i^0 \right] + \rho \sum_i \Re \frac{y_i}{m_i} T$$

where $\Re = 8.314\ \mathrm{J \cdot kg^{-1}\ mole^{-1} \cdot K^{-1}}$. The second term is the sum of the partial pressures of each gas equal to the total pressure, following Dalton's law. By use of the relation

$$y_i = x_i m_i \Big/ \sum_l x_l m_l = \frac{x_i m_i}{m}$$

the total pressure takes the more frequently used form $p = \rho(\Re/m)T$, which is the classical state equation for the mixing of molar mass

$$m = \sum x_1 m_1$$

The internal energy $\bar{\varepsilon}$ being

$$\sum_i y_i \left[\int_0^T C_{vi}\,\mathrm{d}t + Q_i^0 \right]$$

we recover the classical formula $h = \bar{\varepsilon} + p/\rho$. Introducing the energy, $e = \bar{\varepsilon} + u_k u_k/2$, the transport equations for the global density, the momentum, the energy and the mass fractions in a turbulent regime are[6,7]

$$\frac{\partial \rho}{\partial t} + \frac{\partial \rho u_j}{\partial x_j} = 0$$

$$\frac{\partial \rho u_i}{\partial t} + \frac{\partial \rho u_i u_j}{\partial x_j} = -\frac{\partial p}{\partial x_i} + \frac{\partial}{\partial x_j}\left(\tau_{jl} + \tau_{jl}^T\right)$$

$$\frac{\partial \rho e}{\partial t} + \frac{\partial \rho e u_j}{\partial x_j} = -\frac{\partial p u_j}{\partial x_j} + \frac{\partial}{\partial x_j}\left[\left(\tau_{jl} + \tau_{jl}^T\right)u_l\right] - \frac{\partial}{\partial x_j}\left(q_j + q_j^T\right)$$

$$\frac{\partial \rho y_m}{\partial t} + \frac{\partial \rho y_m u_k}{\partial x_k} = -\frac{\partial}{\partial x_k}\left(\rho V_m^k y_m\right) - \frac{\partial}{\partial x_k}\overline{\rho y_m'' u_k''} + \overline{\omega_m}$$

In the last formula, V_m^k is the kth component of the mean velocity of species m relative to the moving frame of the center of mass. Here, y_m'' and u_k'' are the turbulent fluctuations relative to the Favre averages of the corresponding variable and τ_{ij}^T is the Reynolds stress tensor. The correlation terms between turbulent fluctuations in the energy equation, summarized here globally by the generic term q_j^T, are composed of several terms from which we retain generally only the correlation $\overline{\rho u_j'' h''}$, the others being neglected. The first two terms on the right-hand side of the last equation are molecular and turbulent diffusion terms for the various species, the modeling of which will be defined in the following paragraphs. The chemical source term $\overline{\omega}_m$ is equal to zero in this case considering pure diffusion.

We now define the sensible enthalpy h_s, the sensible internal energy e_s, and the equivalent of the ratio of specific heats γ_s (becoming the classical γ when C_p and C_v are constant with temperature) by

$$h_s = \sum_i y_i \int_0^T C_{pi}\,\mathrm{d}t$$

$$e_s = \sum_i y_i \int_0^T C_{vi}\,\mathrm{d}t = h_s - \frac{p}{\rho}, \qquad \hat{\gamma} = \frac{h_s}{e_s}$$

We deduce immediately that $p = (\hat{\gamma} - 1)\rho e_s$. This relation is identical to the fundamental one used in the case of perfect gases when using h_s and e_s in place of h and e. A rigorous modeling of the laminar term of heat transfer is provided by the transport theory of gases.[8] By neglecting the weak term of interspecies heat diffusion, known as the Dufour effect,[8,9] and with use of the following variables, mean specific heat

$$\hat{C}_p = \sum_{m=1}^{N} y_m C_{pm}$$

sensible enthalpy of species m

$$h_{sm} = \int_0^T C_{pm}\,\mathrm{d}t$$

and sensible energy

$$\bar{e} = e_s + u_k u_k/2$$

then, the molecular heat flux q_j takes the form

$$q_j = -\frac{\lambda}{\hat{C}_p}\frac{\partial h_s}{\partial x_j} + \rho \sum_{m=1}^{N} h_m y_m V_m^j + \sum_{m=1}^{N} \lambda \frac{h_{sm}}{\hat{C}p}\frac{\partial y_m}{\partial x_j}$$

By a careful decomposition of the term $\overline{\rho u_j'' h''}$ and with the following three gradient type approximations

$$\sum_{m=1}^{N} \tilde{y}_m \overline{\rho u_j'' h_{sm}''} = -\lambda_T \frac{\partial T}{\partial x_j}$$

$$\rho y_m V_m^j = -\rho D \frac{\partial y_m}{\partial x_j}, \qquad \overline{\rho y_m'' u_j''} = -\rho D_T \frac{\partial y_m}{\partial x_j}$$

the final form that can be retained for the energy balance equation is

$$\frac{\partial \rho \bar{e}}{\partial t} + \frac{\partial}{\partial x_j}(\rho \bar{e} + p)u_j = \frac{\partial}{\partial x_j}\left[\left(\frac{\mu}{Pr} + \frac{\mu_T}{Pr_T}\right)\frac{\partial}{\partial x_j}(\hat{\gamma}\bar{e})\right]$$

$$- \frac{\partial}{\partial x_j}\left[\left(\frac{\mu}{Pr} + \frac{\mu_T}{Pr_T}\right)\frac{\partial}{\partial x_j}\left(\hat{\gamma}\frac{u_k u_k}{2}\right)\right]$$

$$+ \frac{\partial}{\partial x_j}\left[\sum_{m=1}^{N} \frac{h_{sm}\mu}{Pr}\left(1 - \frac{1}{Le}\right)\frac{\partial y_m}{\partial x_j}\right]$$

$$+ \frac{\partial}{\partial x_j}\left[\sum_{m=1}^{N} \frac{h_{sm}\mu_T}{Pr_T}\left(1 - \frac{1}{Le_T}\right)\frac{\partial y_m}{\partial x_j}\right] + \frac{\partial}{\partial x_j}\left[u_k\left(\tau_{jk} + \tau_{jk}^T\right)\right]$$

where the Prandtl and Lewis laminar and turbulent numbers are defined by

$$Pr = \frac{\mu \hat{C}_p}{\lambda}, \qquad Le = \frac{\lambda}{\rho \hat{C}_p D}, \qquad Pr_T = \frac{\mu_T \hat{C}_p}{\lambda_T}$$

$$Le_T = \frac{\lambda_T}{\rho \hat{C}_p D_T}$$

The first of the preceding three gradient type approximations is classically used for modeling turbulent flows.[10] This approximation defines a thermal conductivity for the turbulent fluctuations by analogy with Fourier's law. Using the same kind of analogy, the third approximation is established following the second one, in which the modeling of the transport coefficients for the terms issuing from molecular fluctuations can be established rigorously in the field of the study of the transport of mixing of gases.[8] The modeling of the turbulent transport coefficients in the third approximation is the result of an analogy that considers a turbulent mixing as a gas of pseudoparticles. We now will refine this idea.

Modeling of Interspecies Diffusion in a Turbulent Mixing of Gases

In addition to x_i and y_i, we define the local mean velocity $\boldsymbol{v}_i$ of the molecules of the species i. The mean velocity relative to the center of mass of all of the kinds of molecules is defined as

$$\boldsymbol{u} = \sum_i y_i \boldsymbol{v}_i$$

and the fluctuation of each species relative to this mean is $\boldsymbol{V}_i = \boldsymbol{v}_i - \boldsymbol{u}$. The rigorous theory of molecular transport[8] allows one to establish an equation between these variables and the mean flow terms, the order of precision of these relations being consistent with the Navier–Stokes equations. We use a simplified version of this equation, which neglects the significantly smaller terms.[7,9] The simplified equation can be shown to be

$$\nabla x_i = \sum_{j=1}^{N} \frac{x_i x_j}{D_{ij}} (\boldsymbol{V}_j - \boldsymbol{V}_i) \tag{1}$$

We can use this expression, where the binary diffusion coefficients D_{ij} appear, to establish the general expression of the multicomponent diffusion coefficients used in the calculations. For this purpose, we will also define the velocity fluctuations relatively to the mean molar velocity

$$\boldsymbol{V}_i' = \boldsymbol{v}_i - \sum_j x_j \boldsymbol{v}_j \tag{2}$$

By definition, the multicomponent diffusion coefficient D_i is given by

$$x_i \boldsymbol{V}_i' = -D_i \nabla x_i \tag{3}$$

By use of relations (1–3) and of the linear independence of the vectors $\boldsymbol{V}_i$ and $\boldsymbol{V}_j$, we can derive rigorously the following relation determining coefficients D_i:

$$D_i = \frac{1 - x_i}{\sum_{j \neq i} (x_j / D_{ij})} = \frac{\sum_{j \neq i} x_j}{\sum_{j \neq i} (x_j / D_{ij})} \tag{4}$$

We will now examine the cases where these coefficients can be equated for each i. First, in the case of a binary mixing where there is only one coefficient D_{12}, we immediately have $D_1 = D_2 = D_{12}$. This situation can be extended, with a good approximation, to the case where two families of particles exist, with the diffusion properties close between them. One then considers that the interspecies diffusion coefficient can be reduced to a single binary coefficient between the two families, implying the unity of the multicomponent diffusion coefficient. Another type of situation is the one where a great number of different species coexist in the mixing. Let us write Eq. (4) as

$$\frac{1}{D_i} = \frac{\sum_{j \neq i} (x_j / D_{ij})}{\sum_{j \neq i} x_j}$$

We see that $1/D_i$ equals the mean of the $1/D_{ij}$ of the $N-1$ species different from i. If the number of species is sufficiently high, this mean will vary weakly with i, and we will approach the situation where the multicomponent diffusion coefficient can be considered as equal for all of the species. This remark will be useful in justifying the approximation we will use in our modeling of turbulent diffusion.

An interesting consequence of the equality of the multicomponent coefficients is that the fluctuations of the species relative to the center of masses can be connected to the mass fractions by the same relation as the definition relation (3) connecting the fluctuations relative to the center of molar fractions with the molar fractions.[9] This case, in which we then recover the well-known Fick's law, is a supplementary case, where this law can be considered as rigorous, as in the case of binary mixing.

We will follow a hypothesis such as the one of Reynolds: consider turbulent flow as a gas of particles, these particles being in fact the turbulent eddies that are the basic particles constituting the gas. These particlelike packets, interacting like large molecules, are the cornerstone of the basic analogy hypothesis for determining turbulent shear stresses with the more commonly used concept of turbulent viscosity. We will apply our earlier considerations to this gas of pseudoparticles. These pseudoparticles have variable sizes and, therefore, have a great number of types that are taken to be the species used in establishing the earlier equations, in the case of equality of the multicomponent coefficients. The primitive molecules become indiscernible at the level of turbulent fluctuations and are grouped into big pseudoparticles, whose diffusion properties obey the rule derived in the case of a great number of species. We can then define for the diffusion of these pseudoparticles a turbulent diffusion coefficient available for each molecular species, $y_i V_i = -D_T \nabla y_i$. Concerning molecular transport coefficients, more often very weak in comparison with the turbulent ones, a mean mixing viscosity is used, and gradients of the local composition of the gas are neglected. The Lewis numbers, often shown in previous works to be near unity[7,9] will be taken equal to one. As said before, a majority of turbulence models presently used in computations make the Boussinesq hypothesis to evaluate the effect of turbulent fluctuations on the flow, by analogy with the effects of molecular fluctuations. This reasoning was followed to establish our model of turbulent diffusion. This model is in fact consistent with purely algebraic models or with one or two transport equations models. As examples, we will examine the Baldwin–Lomax model[11] and then the k–ε model with Chien's[12] approximation near the wall.

Turbulence Models

The first turbulence model used in our calculations is the well-known Baldwin–Lomax model.[11] Two versions of the model are used to evaluate eddy viscosity in close proximity to the wall and in the wake. We use the first version, including wall effect, upstream of the base, to evaluate the development of the boundary layer on the fuselage. From the base to the far downstream flowfield, the second version of the Baldwin and Lomax model, available in the case of pure wakes, is used. The effect of the wall in the area restricted to the base is neglected in the absence of a satisfactory low Reynolds correction in the vicinity of this area.

We recall the transport equations of the second model used, which is the k–ε model of Chien,[12] including wall effects.

As in all of the k–ε models, the turbulent viscosity takes the form $\mu_T = C_\mu f_\mu (\rho k^2/\varepsilon)$ where $C_\mu = 0.09$ and $f_\mu = 1 - \exp(-0.0115 y^+)$ with $y^+ = (y - y_p)\sqrt{(\rho_p \tau_p)}/\mu_p$, where index p designates values at the wall. The transport equations then become (in our cylindrical coordinate system)

$$\frac{\partial(\rho k y)}{\partial t} + \frac{\partial(\rho k u y)}{\partial x} + \frac{\partial(\rho k v y)}{\partial y} - \frac{\partial}{\partial x}\left[\left(\mu + \frac{\mu_T}{\sigma_k}\right) y \frac{\partial k}{\partial x}\right]$$

$$- \frac{\partial}{\partial y}\left[\left(\mu + \frac{\mu_T}{\sigma_k}\right) y \frac{\partial k}{\partial y}\right] + \frac{2\mu k}{(y - y_p)^2} y - P_k y - \rho \varepsilon y = 0$$

where $\sigma_K = 1$ and

$$P_k = \frac{4}{3}\mu_T\left[\left(\frac{\partial u}{\partial x}\right)^2 + \left(\frac{\partial v}{\partial y}\right)^2 + \left(\frac{v}{y}\right)^2 - \frac{\partial u}{\partial x}\frac{\partial v}{\partial y} - \frac{v}{y}\left(\frac{\partial u}{\partial y} + \frac{\partial v}{\partial y}\right)\right] + \mu_T\left(\frac{\partial u}{\partial y} + \frac{\partial v}{\partial x}\right)^2 - \frac{2}{3}\rho k\left(\frac{\partial u}{\partial x} + \frac{\partial v}{\partial y} + \frac{v}{y}\right)$$

$$\frac{\partial(\rho\varepsilon y)}{\partial t} + \frac{\partial(\rho\varepsilon u y)}{\partial x} + \frac{\partial(\rho\varepsilon v y)}{\partial y} - \frac{\partial}{\partial x}\left[\left(\mu + \frac{\mu_T}{\sigma_\varepsilon}\right)y\frac{\partial\varepsilon}{\partial x}\right] - \frac{\partial}{\partial y}\left[\left(\mu + \frac{\mu_T}{\sigma_\varepsilon}\right)y\frac{\partial\varepsilon}{\partial y}\right] + \frac{2\mu f_2^*\varepsilon}{(y - y_p)^2}y + 1.8 f_2\rho\frac{\varepsilon^2}{k}y - 1.35\frac{\varepsilon P_k}{k}y = 0$$

where $\sigma_\varepsilon = 1.3$, $f_2^* = \exp(-0.5y^+)$ and $f_2 = 1 - \frac{2}{9}\exp[-(R_T^2/36)]$ with $R_T = \rho k^2/\mu\varepsilon$.

In the same spirit as in the case of Baldwin–Lomax model,[11] the Chien model[12] is used downstream of the base by canceling the correcting terms in $1/(y - y_p)^2$ in the equations and by equating the damping factor f_μ to 1.

Numerical Scheme

The numerical scheme used in the NASCA code is an extension of the Osher and Chakravarthy scheme[13] to the case of a mesh that can be locally nonuniform. The resulting numerical code is totally implicit, including its modules treating the turbulence transport. To test the ability of the code to precisely simulate separated flows while eliminating the uncertainties coming from the turbulence model itself, the scheme was first validated using a hypersonic laminar flow.[14] The implementation of the k–ε model in a fully implicit scheme is not straightforward and necessitates theoretical preconditioning.[15]

III. Application of the Method on a Test Case

Basic Test Case and Validation in Cold Air/Air Conditions

The aim of the experimental study that provided the test case chosen here was to furnish a detailed experimental data benchmark on the velocity and Reynolds stress fields in the vicinity of the base and at the birth of the wake of a simplified afterbody equipped with a cold air secondary jet.[15] This data benchmark was later used to validate several Navier–Stokes codes.[16] The Mach number of the external flow is 4.18, the total pressure and total temperature are 10^6 Pa and 300 K, respectively. For the propulsive jet, the corresponding values are 3.45, 4.23×10^6 Pa and 300 K, respectively, corresponding to a pressure ratio $P_{tj}/P_{\text{ext}} = 814$. Experimental data for such a test case with realistic total temperatures of the propulsive jet (2000–3000 K) and realistic chemical composition of the secondary flow (for instance, gases issued from the combustion of a propergol) are presently lacking. The measurement techniques for these physical properties (chemical composition and temperature fields) are still being improved. The problem of the degree of confidence in the physical reality of the model is important. The basic model of turbulent diffusion used here has been previously tested in calculations using multicomponent methods[17,18] that consist of coupling the perfect external fluid flow with a simplified analytical representation of the mixing layer. We recall that these methods of calculation that were implemented in the past, at a time when Navier–Stokes codes were not yet used, quickly evaluated mean pressure and temperature considered as weakly varying in the recirculating zone of a base flow. These methods were extended to the case of injection of reactive gaseous species at the base. The degree of confidence of these methods was extensively tested,[17,18] and the results given by the model of turbulent diffusion in the case of a base bleed was validated satisfactorily, in the context of these approximate methods, by comparison with experimental data[19,20] that furnished base pressure evolution with respect to the injection of helium or argon. Some of these experiments also considered the effects of heating the injected argon at 3000 K (Ref. 19). Next, we verified that results given by the multicomponent methods in predicting the uniform pressure, temperature, or concentration in the recirculating zone approximated, with a maximal shift of 10%, mean values of the same data given by Navier–Stokes computations in cases of base flows with propulsive jets. Experimental results are not available in these cases; therefore, the preceding considerations have been our guide for generalizing the model of turbulent diffusion to Navier–Stokes codes and evaluating tendencies in the evolution of aerothermal fields. Before performing prospective computations in such cases, a validation of the solver in air/air conditions where experimental data exist is necessary.

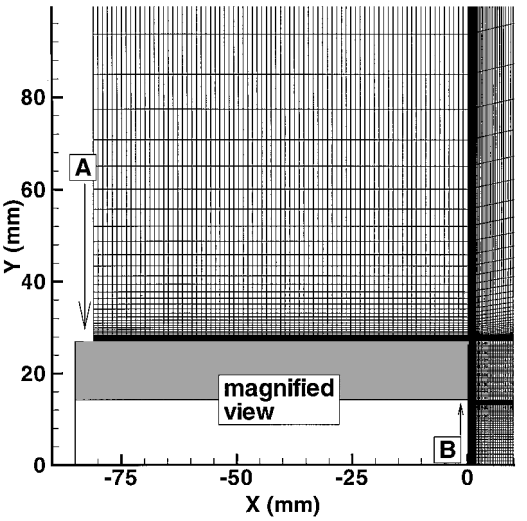

Fig. 1 Computational grid, mesh 2: 201 × 145 points.

The mesh chosen for the computation with NASCA is shown in Fig. 1, where the shape of the simplified afterbody is also shown. This afterbody was equipped with an adapted nozzle whose very thin exit boundary layer was partially measured with a pitot probe and imposed as incoming jet flow in our supersonic calculation. The external boundary layer, 81 mm upstream of the base, was measured with a pitot probe and imposed as the upstream inflow condition. The use of pitot probes for the determination of the boundary layer is necessitated by the precision of the calculation requiring the knowledge of points in a very close proximity to the wall that cannot be accessed by laser Doppler velocimetry (LDV). The two flows imposed as upstream boundary conditions on sides A and B of the mesh (Fig. 1) are assumed to be fully turbulent. The incoming profiles required for the calculation are entirely deduced from the pitot probe data, the Crocco hypothesis, and an evaluation of the viscosity with the Baldwin and Lomax model.[11] When the k–ε calculation is performed, the evaluation of the corresponding profiles of k and ε is deduced from the Baldwin and Lomax viscosity and the Bradshaw hypothesis, $u'v' = -0.3k$. The computational mesh consists of 201 points in the X direction and 145 points in the Y direction, with a thinning of the grid lengths in directions normal to the walls determined after a careful analysis of spatial convergence.[15] This research of spatial convergence was made, essentially, in two steps, with the criterion, verified in preceding numerical studies, that the data that are most sensitive to the mesh are the wall pressures. In the first step, the optimal cell width in the X direction was researched at the base by calculations using variable ratios of geometrical progression from the wall. The pressure at the wall was found to be independent of ratios up to 1.05, which was the adopted value. The second step examined the effect of the width of the mesh in the Y direction, at the level of the incoming external boundary layer. Results of this study are shown in Fig. 2. The data obtained with mesh 1 and a mesh eight times thinner in the boundary layer (mesh 2) reveal a sensitivity of 6% in the k–ε results and much larger in the Baldwin and Lomax calculation.[11] All other calculated data at mesh points not situated on the wall presented variations lower than 1% with both models. Previous studies have shown that the mesh refinement in the very thin internal boundary-layer area is sufficient, and its influence is not important; therefore, in the present study,

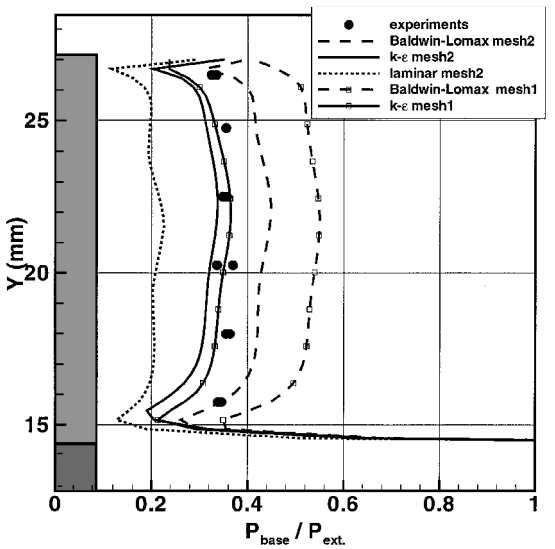

Fig. 2 Base static pressure; air $T_{tj} = 300$ K.

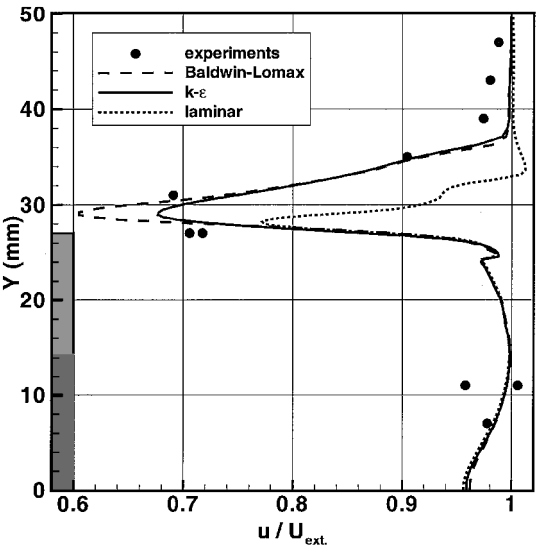

Fig. 4 Longitudinal velocity profiles at $X = 40$ mm; air $T_{tj} = 300$ K.

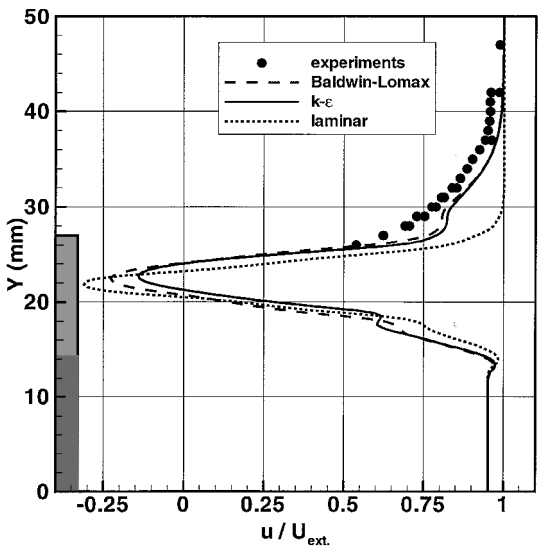

Fig. 3 Longitudinal velocity profiles at $X = 4$ mm; air $T_{tj} = 300$ K.

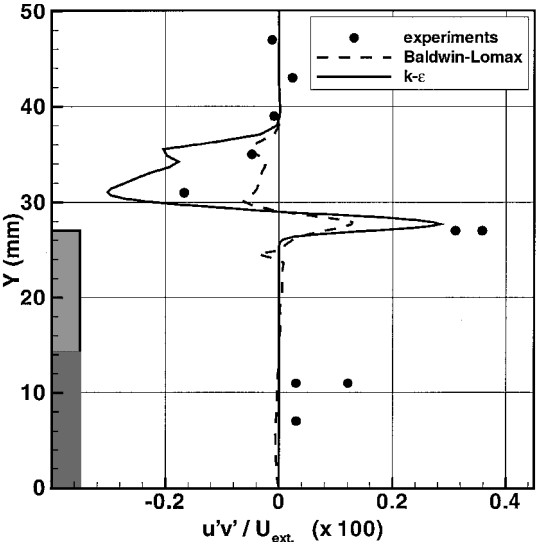

Fig. 5 Turbulent shear stress profiles at $X = 40$ mm; air $T_{tj} = 300$ K.

mesh refinement has been restricted to the external boundary-layer region. The study of spatial convergence has been limited to the reference case of cold flow, air–air conditions, and mesh 2 has been retained for performing all of the following computations. Results obtained in the same conditions with a laminar flow are also shown, for comparison, in Figs. 2–4.

The curves representing the calculated pressures show notable differences between the levels predicted by the Baldwin–Lomax[11] and the k–ε models. The base pressures appear to be better predicted by the last one, discrepancies can attain 30% near the lower and upper sides of the base, at the level of the separation of incoming boundary layers, but in the largest part of the base, pressure is predicted with a confidence interval of 6% (Fig. 2). Notice an important dispersion of the experimental data, due to uncertainties in fixing stagnation pressure in different runs of the ONERA wind tunnel R2Ch. The maximal dispersion (10%) is shown in Fig. 2 by two points at the same Y ordinate. The prediction of the base pressure remains a major challenge in the calculation of base flows. Previous calculations with k–ε models,[21–23] performed in the case of flows without propulsive jets, have shown also discrepancies in the prediction of base pressure. The same observation has been made in recent calculations of base flows/plume interaction.[24,25] To our knowledge, the assurance of predicting mean base pressures with a confidence interval of ±10% is not presently established when standard models are used. The precision of the imposed experimental boundary layer at −81 mm allowed a good reproduction of the external boundary layer up to the separation point at the level of the base. Field measurements downstream of the base were all performed with LDV, and the comparisons with calculated values show a good agreement between calculation and experiment for the determination of axial velocities at 4 mm downstream of the base (Fig. 3). Farther downstream, at $X = 40$ mm, in the interaction area between the jet and the external flow (Fig. 4), the predictions remain satisfactory with an advantage for the k–ε model. Concerning the prediction of the turbulent shear stresses (Fig. 5), in this downstream area, a greater extension of measurement results allows one to notice a correct prediction of mean and fluctuating values by the k–ε model, even if noticeable scatter of experimental values is visible in Figs. 4 and 5 in the vicinity of $Y = 10$ and 30 mm.

After having validated the NASCA code with cold propulsive jet, we are now in position to perform prospective calculations of the effects of diffusion of propulsive species different from the external air and of the effect of realistic high-level temperatures characterizing the propulsive flow.

Prospective Calculations with a Propulsive Jet Composed of Propergol Combustion Species

Up to a static temperature of 2500 K, the reactions of dissociation of air can be neglected and in fact, this reactivity is not very important up to approximately 3000 K. In the domain of temperature

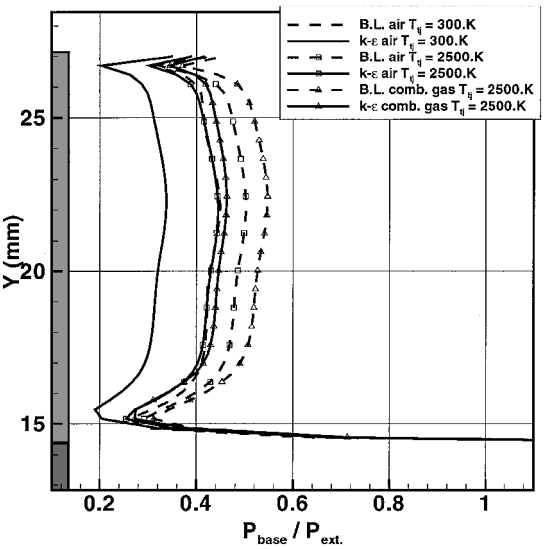

Fig. 6 Base static pressure; T_{tj} = 300 and 2500 K.

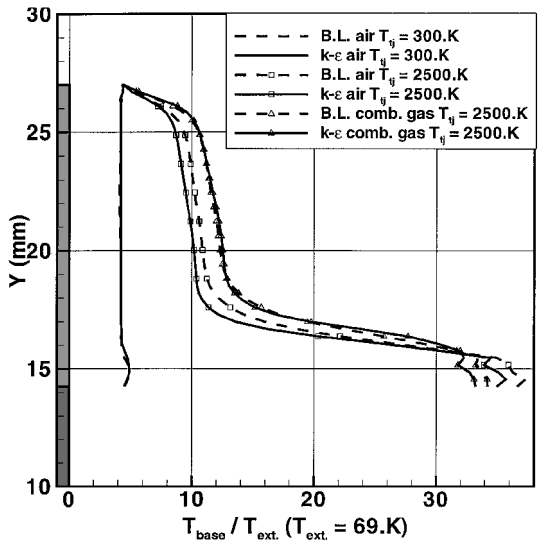

Fig. 7 Base static temperature; T_{tj} = 300 and 2500 K.

levels provided by usual propulsive jets, recombustion in the base area is not often observed, and it has never been observed in experimental cases using powder impulse jets. For these reasons, we treat propelled afterbody flows in pure diffusion as realistic cases at a jet total temperature of 2500 K. We choose for our calculations the basic test case with the same geometric configuration and calculation grid. First calculated as a hot air jet, the propulsive jet is composed next, in mass fractions, of the following species, issuing from propergol combustion: CO 6.8%, CO_2 26.6%, HCL 27.3%, H_2 0.5%, H_2O 28.2%, and N_2 10.6%.

The evolutions of the base pressure for a jet stagnation temperature of 2500 K, compared with the cold air–air case, are shown in Fig. 6. We have noticed, in the preceding calculations, that the presence of different species in the propulsive jet is practically ineffective on the base pressure level at low jet stagnation temperatures. This base pressure increases progressively with the jet stagnation temperature level and becomes significant at 2500 K (Fig. 6). The amplification effect due to the nature of the species composing the jet is more important when predicted with the algebraic model. Contrary to the base pressure, base temperature is predicted in a rather good agreement by the two turbulence models, as shown in Fig. 7. In the vicinity of the interior corner of the base, near the nozzle exit, we can see the peak of static temperature that could be the origin of recombustion phenomena. As for base pressures, the nature of the propulsive jet does not induce large differences on base temperatures at low jet stagnation temperatures.

We will now examine the thermal ambiance of the missile afterbody, which is very important for the problem of infrared detection, for a jet stagnation temperature of 2500 K. In Figs. 8 and 9, we observe that the main high-temperature regions other than the near jet core are the external lip of the nozzle and the reflection point of the barrel shock on the axis. The interior of the barrel is characterized by low-temperature zones near the axis (dark blue zones in Figs. 8 and 9). The heated fluid at the lip of the nozzle, whose temperature level is practically the stagnation temperature of the nozzle flow, is convected far downstream in the mixing layer separating the external flow and the propulsive jet, constituting the hot envelope observed in Figs. 8 and 9. The length of this envelope, where static temperature reaches levels higher than 500 K, is of the order of the missile length. The Baldwin–Lomax model[11] predicts a notably larger hot envelope than the k–ε model (Fig. 8). The two models are in good agreement for the determination of the temperature level attained by the second hot zone downstream of the reflection point. This level is greater than 700 K in the more realistic case of a jet composed with propergol species; the models agree, too, in the prediction of the spatial extension of this zone. The mixing boundary stays at a level higher than 500 K until a zone where it joins the hot flow downstream

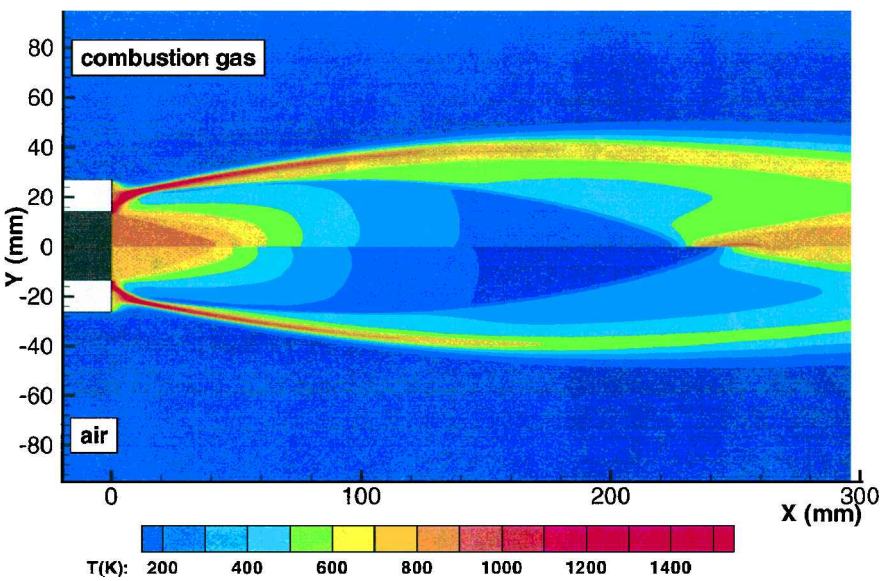

Fig. 8 Static temperature levels with Baldwin–Lomax[11] turbulence model; T_{tj} = 2500 K.

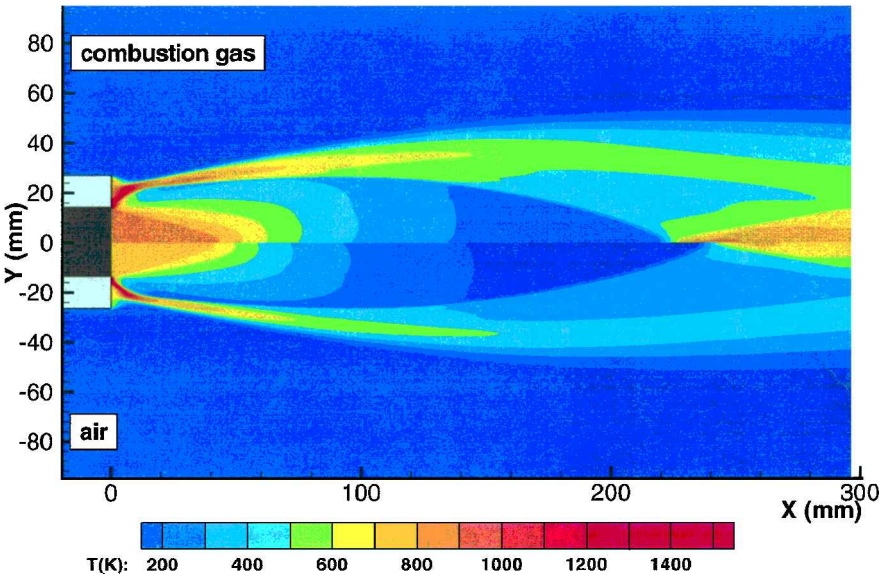

Fig. 9 Static temperature levels with k–ε turbulence model; T_{tj} = 2500 K.

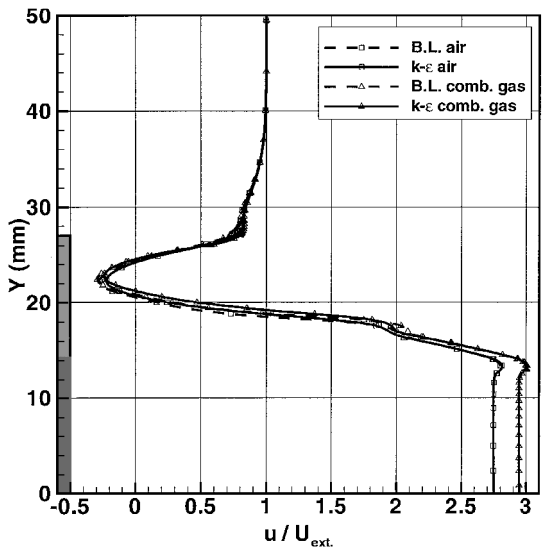

Fig. 10 Longitudinal velocity profiles at X = 4 mm; T_{tj} = 2500 K.

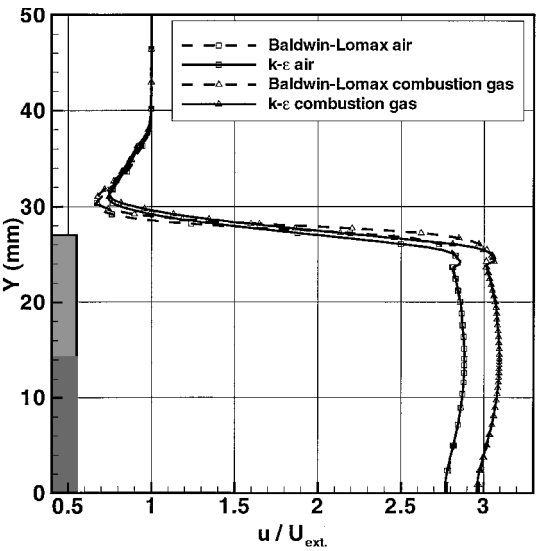

Fig. 11 Longitudinal velocity profiles at X = 40 mm; T_{tj} = 2500 K.

of the reflection point to generate a wake at a temperature level of the order of 600–700 K in the case of propergol propulsive jet. Here, too, the Baldwin–Lomax model[11] predicts a stronger heating of the mixing boundary and the same level of heating downstream of the barrel shock reflection, this second heating being generated by nonviscous mechanisms. In any case, the simulation of realistic conditions predicts a considerable extension of the hot zones in the afterbody flow when compared with the missile's dimensions.

The velocity profiles, shown in Figs. 10 and 11, at x = 4 and 40 mm after the base, respectively, confirm that the two models are in agreement when predicting the main flow features (in particular the localization of the barrel shock). This can also be seen in the temperature fields of Figs. 8 and 9. The viscosity has a minor effect in determining this structure, which constitutes the nonviscous skeleton of the flow. The effect of the jet temperature is limited to the area situated between the axis and the mixing layer. The mixing zone constitutes a limit for the penetration of heat coming from the jet. The growth of velocity gradients in the mixing layer with the jet temperature is amplified by the presence of propergol species in this propulsive flow (Figs. 10 and 11) and is a consequence of its growing level of velocity with temperature and species. The level of Reynolds shear stresses (Fig. 12), is not considerably modified by the presence of combustion gas. There are, therefore, no spectacular

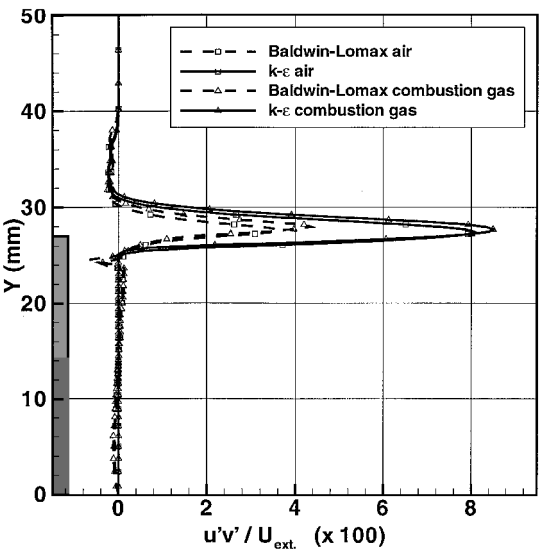

Fig. 12 Turbulent shear stress profiles at X = 40 mm; T_{tj} = 2500 K.

effects of temperature on the dynamic fields and a moderated amplifying effect of the species on the velocity levels in the jet and mixing layer (lower than 10% of the velocity level).

IV. Conclusion

The knowledge of missiles' performance modifications between tests in wind tunnels, often in purely aerodynamic conditions, and real flight tests, where the propulsive jet is composed of combustion species, is still embryonic. A low-cost approach for determining aerothermal data of afterbody flows has been used with the NASCA Navier–Stokes code in the case where the species of the jet are chemically frozen. After a validation in cold air/air conditions, prospective calculations were performed on the same geometric configuration, but with a propulsive jet composed of gases issuing from the combustion of a propergol. A total jet temperatures of 2500 K allowed us to examine heating effects on the near-wake temperature field. The effect of the chemical composition on the near-wake heating has been found to be significant. The results given with a purely algebraic turbulence model (the Baldwin–Lomax model) and a model with two transport equations (k–ε model of Chien) were compared. A first result of this study was to show, theoretically, the coherence between modeling turbulent transport of the species with Fick's law and the use of an eddy viscosity, typical of standard two equation models. A second result was the important variation between turbulence models for establishing values of base pressure and temperature fields in the near wake. Other k–ε models, now available in the NASCA code, will be used during future studies, and it is hoped that future developments of the code will allow us to perform calculations with reactive species, including in particular the prediction of chemical effects such as the occurrence of recombustion near the engine afterbody. This kind of aerothermal problem is a future challenge for the improvement of turbulence models.

Acknowledgments

This work was supported by the French "Direction des Systèmes de Forces et de la Prospective" (DGA/DSP) for the theoretical study and by Aérospatiale for the experiments.

References

[1]Sahu, J., "Computations of Supersonic Flow over a Missile Afterbody Containing an Exhaust Jet," AIAA Paper 85-1815, Aug. 1985.

[2]"Flow Past Missile Afterbodies," Group for Aeronautical Research and Technology in Europe, TP 061, Action Group 09 Final Rept., Nov. 1991.

[3]"Aerodynamics of 3-D Aircraft Afterbodies," AGARD Advisory Rept. No. 318, Sept. 1995.

[4]Servel, P., Reijasse, P., Benay, R., and Corbel, B., "Etudes fondamentales sur les aspects aérodynamiques et thermiques des écoulements à l'arrière-corps des missiles," *Missile Aerodynamics*, RTO Meeting Proceedings 5, NATO, 1998, pp. 18.1–18.14.

[5]McBride, B. J., Gordon, S., and Reno, M. A., "Coefficients for Calculating Thermodynamic and Transport Properties of Individual Species," NASA TM 4513, 1993.

[6]Jones, W. P., "Turbulence Modeling for Combustion Flows," *Modeling of Combustion and Turbulence*, Von Kármán Inst. Lecture Series 1992-03, Von Kármán Inst., Rhode Saint Genèse, Belgium, March 1992.

[7]Kuo, K. K., "The Conservation Equations for Multicomponent Reacting System," *Principles of Combustion*, Wiley, New York, 1986, pp. 161–227.

[8]Hirschfelder, J. O., Curtiss, C. F., and Bird, R. B., *Molecular Theory of Gases and Liquids*, Wiley, New York, 1964, Chaps. 7 and 8, pp. 441–610.

[9]Williams, F. A., *Combustion Theory*, Addison Wesley Longman, Reading, MA, 1985, Appendix E, pp. 628–649.

[10]Michel, R., "Equations générales des couches limites," *Couches limites frottement et transfert de chaleur*, Ecole Nationale Supérieure de l'Aéronautique et de l'Espace, Toulouse, France, 1972, pp. 19–29.

[11]Baldwin, B. S., and Lomax, H., "Thin Layer Approximations and Algebraic Model for Separated Turbulent Flows," AIAA Paper 78-0257, Jan. 1978.

[12]Chien, K. Y., "Prediction of Channel and Boundary-Layer Flows with a Low-Reynolds-Number Turbulent Model," *AIAA Journal*, Vol. 20, No. 1, 1982, pp. 33–38.

[13]Osher, S., and Chakravarthy, S., "Very High Order Accurate TVD Schemes," Inst. for Computer Applications in Science and Engineering, Rept. 84-44, Hampton, VA, Sept. 1984.

[14]Chanetz, B., Benay, R., Bousquet, J.-M., Bur, R., Pot, T., Grasso, F., and Moss, J., "Experimental and Numerical Study of the Laminar Separation in Hypersonic Flow," *Aerospace Science and Technology*, No. 3, 1998, pp. 205–218.

[15]Benay, R., and Servel, P., "Applications d'un code Navier–Stokes au calcul d'écoulements d'arrière-corps de missiles ou d'avions," *La Recherche Aérospatiale*, No. 6, 1995, pp. 405–426.

[16]Charmant, S., and Cambier, L., "Calculs d'écoulements compressibles turbulents autour d'arrière-corps avec tuyère," ONERA, TP 1994-68, 1994.

[17]Reijasse, P., Benay, R., Délery, J., and Lacau, R. G., "Missile and Projectile Base-Flow Prediction by MultiComponent Methods," AIAA Paper 88-4380, Aug. 1988.

[18]Reijasse, P., Benay, R., Délery, J., and Lacau, R. G., "Prévision des écoulements au culot de missiles ou de projectiles par des méthodes multicomposant," *La Recherche Aérospatiale*, No. 4, 1989, pp. 15–32.

[19]Bowman, J. E., and Clayden, W. A., "Boat-Tailed Afterbodies at Mach 2 with Gas Ejection," *AIAA Journal*, Vol. 6, No. 10, 1968, pp. 2029, 2030.

[20]Calarese, W., "GAU-8 Projectiles Afterbody Drag Reduction by Boattailing and Base Injection with Heat Addition," AIAA Paper 79-0146, 1979.

[21]Berner, C., and Rozon, B., "Axisymmetric Base Flow Investigation Measurements and Computation," Institut de Recherches Franco-Allemand de Saint-Louis, ISL CO 232/92, Saint-Louis, France, Oct. 1992.

[22]Sahu, J., "Numerical Computations of Supersonic Base Flow with Special Emphasis on Turbulence Modeling," AIAA Paper 92-4352, Aug. 1992.

[23]Espina, P. I., and Piomelli, U., "Validation of the NPARC Code in Supersonic Base Flows," AIAA Paper 97-0032, 1997.

[24]Matesanz, A., Velazquez, A., Perales, J. M., and Santiago-Prowald, J., "Numerical Simulation of Base-Flow/Plume Interaction," AIAA Paper 98-1597, 1998.

[25]Bannink, W. J., Houtman, E. M., and Bakker, P. G., "Base Flow/Underexpanded Exhaust Plume Interaction in a Supersonic External Flow," AIAA Paper 98-1598, 1998.

M. Sichel
Associate Editor

Color reproductions courtesy of ONERA.